IEEE Access
Multidisciplinary | Rapid Review | Open Access Journal

Received July 2, 2021, accepted July 17, 2021, date of publication July 26, 2021, date of current version August 2, 2021.

Digital Object Identifier 10.1109/ACCESS.2021.3099055

Green HSR Reliable Communication With LTE-R Using MIMO-DPD

ANURAG VIJAY AGRAWAL, (Member, IEEE), AND MEENAKSHI RAWAT, (Member, IEEE)
Department of Electronics and Communication Engineering, Indian Institute of Technology Roorkee, Roorkee, Uttarakhand 247667, India

Corresponding author: Anurag Vijay Agrawal (anurag.v.agrawal@gmail.com)

This publication is an outcome of the Research & Development work undertaken in the project under the Visvesvaraya PhD Scheme of Ministry of Electronics & Information Technology, Government of India, being implemented by Digital India Corporation and IMPRINT-II, India under Grant IMP/2018/001569.

ABSTRACT Reliable and efficient High-speed Railways (HSR) is the key component to the concept of Green Smart Cities to combat the prevailing traffic congestion on roads and increasing greenhouse gases in the atmosphere. It is also a fast, safe, and economical transport medium. Long Term Evolution – Railways (LTE-R), though in the developing stage, is a new wireless communications standard for providing intelligent broadband communication services to passengers and train operators. Reliable HSR communication requires more base stations (BSs). The radio frequency power amplifier (RFPA), an integral part of the BS, dominates the overall energy consumption and is inherently nonlinear. Digital Predistortion (DPD), the ultimate Green communication technique, is used to linearize RFPAs and provide less power waste. Multiple-input-multiple-output (MIMO) schemes have been used to achieve enhanced data throughputs and superior transmission reliability. This paper analyzes the effect of DPD arrangement corresponding to these schemes for reliable HSR communication in infrastructure-to-train and inside-station scenarios. The authors consider downlink transmission for the LTE-R specifications at different train speeds. Furthermore, the paper proposes an analytical framework to evaluate the performance of the complete HSR MIMO communications system. This analytical framework characterizes the antenna effects on the Block Error Rate (BLER) and throughput by adopting various transmission modes, viz. SISO, MISO, SIMO and MIMO. Numerical analyses and simulations for the proposed system illustrate better reliability and high throughput performances with higher-order MIMO configurations. Moreover, significant energy savings can be realized by universally deploying DPD across the HSR network in Smart Cities.

INDEX TERMS BLER, DPD, HSR, intelligent transportation, LTE-R, MIMO, nonlinearities, RFPA, smart cities, throughput.

I. INTRODUCTION

Today cities are home to more than 50% of the world's population in comparison to 30% in 1950 [1]. The outcome is the expansion of cities across the globe, which forces governments to act in the direction to enhance facilities and infrastructure in the cities. This situation may require intelligent and sustainable environments to offer citizens a high quality of life, which is regarded as the evolution of Smart Cities. The core infrastructure within a Smart City would include efficient urban mobility and public transport with robust Information and Communication Technology (ICT) connectivity and digitization. One of the International Telecommunication Union (ITU) study groups SG5 focused on sustainable Smart Cities and provisioned ICT as a remedy to economic/environmental problems in urban localities [2].

Railway transportation systems provide perfect fast, safe, economical, and green solutions to various global problems, viz. traffic congestion on roads and carbon dioxide (CO_2) emissions in the atmosphere [3]. Further, the demand for long-distance rail journeys paves the way for High-speed Railways (HSR) for providing low-cost and high convenience benefits to the citizens. The popularity of HSR makes train operators and passengers keen to further demand for the introduction of intelligent transportation services during the train journey. These services improve the safety measures provided during travelling and make the best utilization of railway network infrastructure.

Conventional standards, like the Global System for Mobile Communications – Railways (GSM-R), lag in providing modern transport broadband services like on-board railway

The associate editor coordinating the review of this manuscript and approving it for publication was Pietro Savazzi.

This work is licensed under a Creative Commons Attribution-NonCommercial-NoDerivatives 4.0 License.
For more information, see https://creativecommons.org/licenses/by-nc-nd/4.0/

video surveillance and real-time track monitoring; and public services like mobile ticketing, live streaming, and cellular phone services and provide only low data rate services like dispatching, shunting, and maintenance. Subsequently, Long Term Evolution – Railways (LTE-R) emerges as a new wireless communications standard, still under development, to serve modern HSR systems.

LTE-R has been able to provide better data throughput rates even in high mobility operations and allows devices to maintain a reliable data network connection in a fast-moving train. Additionally, the complementary relationship between multiple-input-multiple-output (MIMO) and Orthogonal Frequency Division Multiplexing (OFDM) schemes makes a MIMO-OFDM system most suitable to be used within LTE-R standard for HSR communications [4]–[6].

Though modern complex modulation schemes are spectrally efficient, a high peak-to-average power ratio (PAPR) puts challenge for base stations (BSs) to achieve efficient radio transmission capabilities in terms of energy efficiency. The radio frequency power amplifier (RFPA) is one of the most expensive and power consumable components in the BS [7]–[9], and the energy consumption of a BS can be reduced by improving RFPA's design. This reduction may be achieved by allowing the RFPA to operate in saturation to fulfill the exact spectrum and power efficiency requirements. Unfortunately, the RFPA behaves nonlinearly in the saturation region and produces distortion to the transmitted signal. As HSR users worldwide need additional BSs along newer rail tracks to avail various high-speed and reliable intelligent transportation services, more RFPAs will be required. These additional RFPAs may give rise to more power consumption within the wireless communication network. Today, multiple antenna configuration-based transceivers are viable solutions to the requirements of enhanced system capacity and superior throughput rates in modern practical wireless communication structures. However, each transmit path has its own RFPA; therefore, efficient usage of RFPAs becomes a crucial aspect in MIMO communication systems.

The RFPA nonlinearity can be dealt effectively with digital predistortion (DPD), which is the most prevalent technique for compensating RFPA non-linearization. The DPD introduces a nonlinear digital model before RFPA to predistort the transmitted signal. This, in turn, cancels the distortion produced by RFPA. There is extensive literature available on the usage of DPD for improving the transmitter's performance by the linearization of transmitter nonlinearities [10]–[13]. However, the focus in the established DPD literature is on analyzing the transmitted signal quality [14]–[17], which does not quantify the capability of the complete communication system. The existing literature reports the impact of linearization using DPD in terms of normalized mean square error (NMSE) and adjacent channel power ratio (ACPR) [18], [19]. NMSE and ACPR are transmitter quality parameters. They do not give any inkling for the energy saved/ throughput achieved for complete communication.

In contrast to the existing research, our work quantifies the effect of RFPA nonlinearity and its linearization with efficiency enhancement using DPD for the complete communication system, including transmitter and receiver. In addition, the paper includes an end-to-end mathematical analysis to evaluate the performance of a practical HSR communication system using MIMO-DPD architecture in terms of signal-to-noise power ratio (SNR) over the dynamic multipath channel. This analytical framework characterizes the antenna effects on the Block Error Rate (BLER) and throughput by adopting various transmission modes, viz. SISO, MISO, SIMO and MIMO. The paper paves the way for achieving Green communications in a high mobility scenario.

The paper is structured as follows. The LTE-R architecture is discussed in Section 2. The section also includes a brief comparison among GSM-R, LTE, and LTE-R. Section 3 includes discussion on the adaptation of MIMO and DPD technologies for green and reliable HSR communications. Section 4 describes the system model. This section presents the end-to-end mathematical analysis of the complete communication system. The section also includes the assumptions taken for the present study. Section 5 consists of the results and discussion of the measurements. Finally, Section 6 concludes the paper.

II. LTE-R ARCHITECTURE

Various transport data communication standards use Intelligent Transportation System (ITS) applications to realize a safe HSR operation [20]. In 2016, 60 countries on five continents were using GSM-R. However, recently, several operators of mass transit systems based on communication-based train control (CBTC) and GSM-R determine to move to LTE-R [21], [22]. Following the user requirement, Future Railway Mobile Communications System (FRMCS) will take place on 3rd Generation Partnership Project (3GPP) based 5G communication solutions [23]. LTE-R is expected to offer high data rate services both for passengers and trains. These services may be implemented in two important scenarios – (1) during high-speed train movement, known as an infrastructure-to-train scenario, and (2) when the train is in a stationary position or at very low speed within the railway station platform limits, known as an inside-station scenario.

LTE-R is a railway communication standard based on the existing LTE system architecture. It supports packet-switching in contrast to the circuit-switching arrangement of the GSM-R model. LTE-R provides a reliable Internet Protocol (IP) connection between the passenger's user equipment (UE) and the packet data network (PDN) to access the broadband communication applications without any disruption in both scenarios. LTE-R differs from the conventional LTE networks in terms of architecture, system parameters, network layout, types of services, and the quality of service [24]. Table 1 summarizes the performance comparison specifications for GSM-R, LTE, and LTE-R.

The conventional LTE architecture consists of two networks: Evolved Packet Core (EPC) and Radio Access

TABLE 1. GSM-R, LTE-R and LTE specifications.

Parameters	GSM-R	LTE-R	LTE
Frequency bands	GSM 450/480/850/900, DCS 1800, PCS 1900	LTE 700/800/900/1500/ 1700/1800/2100/2600	LTE 800/1800/2600
Data rate	< 200 kbps	> 2 Mbps	≤ 25 Mbps (for uplink), ≤ 75 Mbps (for downlink)
Bandwidth	0.2 MHz	≥ 10 MHz	1.4 MHz – 20 MHz
Modulation Scheme	Gaussian MSK	QPSK, 16QAM, 64QAM	16QAM, 64QAM, 128QAM
Multiplexing Scheme	TDMA	OFDMA, SC-FDMA	OFDM
Signal transmission	Circuit- Switched	Packet- Switched (UDP- based)	Packet-Switched
Data Packet retransmission	No	Yes (UDP- based)	Yes (IP-based)
Antenna Configuration	SISO	MIMO	MIMO, Massive MIMO
All IP (native)	No	Yes	Yes
Market support	Until 2025	Yes, Building standards	Yes, Matured

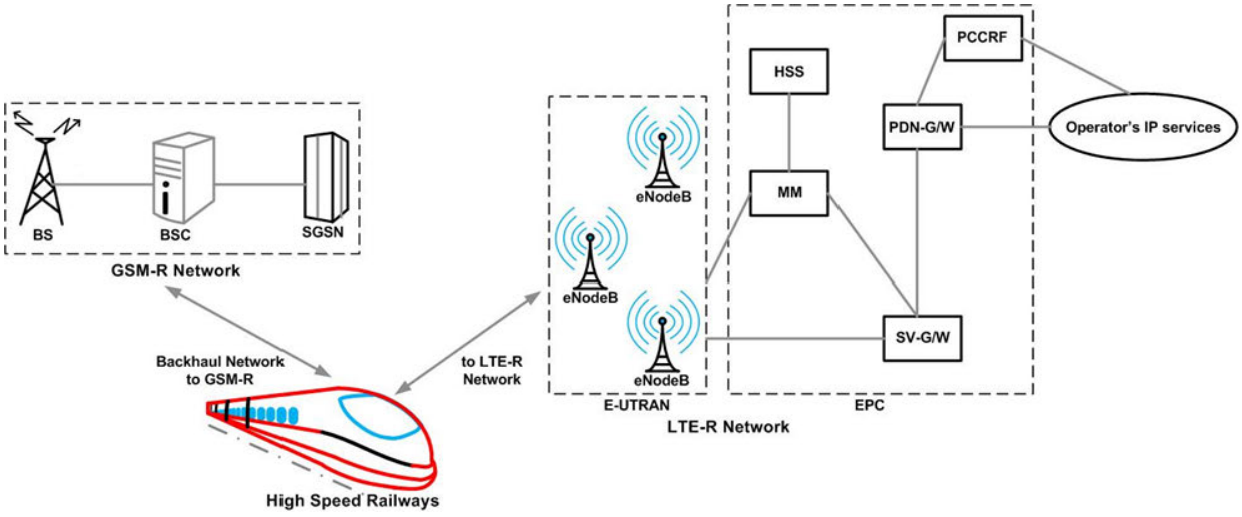

FIGURE 1. Reference architecture for LTE-R communications.

Network (RAN). The access network is known as Evolved Universal Terrestrial Radio Access Network (E-UTRAN) in LTE-R. The evolved Node BS (eNodeB), a part of the E-UTRAN, is the component that allows UE to connect to the LTE-R network. The EPC is the LTE-R core network and performs functions like mobility management, authentication, quality of service, routing upload and download IP packets, IP address allocation, and more. EPC supports seamless handovers to eNodeBs, and each E-UTRAN cell maintains high data/voice capacity by high-speed packet access (HSPA) technology. LTE-R provides an additional radio access system to match HSR-specific needs. This extra radio system offers traffic safety services by exchanging transmission signals with on-board units. The architecture of LTE-R [25], as presented in Fig. 1, incorporates aspects of the HSR communications management policy. Various logical nodes and functions used in LTE-R architecture are: Policy Control and Charging Rules Function (PCCRF), Home Subscriber Server (HSS), PDN Gateway (PDN-G/W), Serving Gateway (SV-G/W), and Mobility Management Entity (MM) [26].

The PCCRF provides the bit rate information and matches a specific data flow with the user's subscription profile, thus helps in policy decision-making. HSS holds information about PDNs and helps the PDNs to connect with UE. PDN-G/W serves as the mobility anchor for interworking with non-3GPP technologies and is responsible for allocating IP addresses to the users and filtering these user IP packets during downlink transmission. The SV-G/W collects the information for call charges in the visiting network and arranges call interceptions as per existing laws in the country. MM processes signaling between the eNodeB and UE to have a successful downlink transmission.

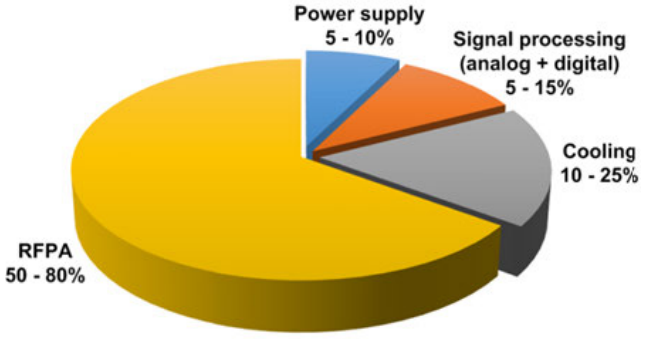

FIGURE 2. BS power consumption.

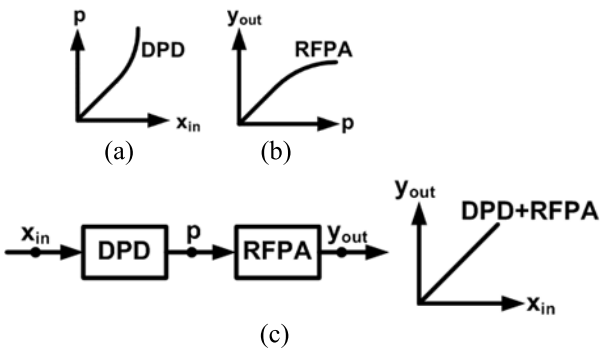

FIGURE 3. The DPD concept: input-output characteristics. (a) DPD, (b) RFPA, (c) (DPD+RFPA).

III. MIMO-DPD: THE WAY TO GREEN AND RELIABLE HSR COMMUNICATIONS

The increasing emission of greenhouse gases in the atmosphere is causing global warming. It is estimated that the global energy consumption of ICT industries is about three percent of the worldwide energy consumption, which is equivalent to about two percent of the global CO_2 emissions. Wireless communication networks contribute about twelve percent of ICT emissions, whereas the largest fraction of energy consumption within these networks is due to BSs. Moreover, HSR users worldwide need additional BSs along newer rail tracks to support high mobility lifestyle 'always get connected' and to avail various high-speed and reliable broadband services. The added BSs may account for the sudden increase in greenhouse gases and pollution with the additional energy costs to operate them.

The rising energy costs and carbon footprint of operating cellular communication systems have stimulated the researchers to work in an innovative research area known as ''Green Communications''. The notion of ''Green technology'' in cellular communication systems is meaningful with a point of view of energy-saving and performance analysis of various components in the communication system. This saving not only provides economic benefits (lower energy costs) but better practical usage (increased battery life in mobile devices and less heat dissipation at BSs) also. The MIMO-DPD combination can efficiently address the crucial issue of high energy dissipation within the BSs.

MIMO technology has emerged as one of the remarkable innovations utilized to fulfill the higher data throughput rates and communication reliability demands for modern and future wireless communications. However, MIMO configuration requires more hardware components. It needs additional RFPAs, couplers, and antennas on the transmitter side; whereas at the receiver side, it needs additional antennas, couplers, and low-noise amplifiers (LNAs) [27]. Unfortunately, the RFPAs are inherently nonlinear and consume a substantial amount of power within the BSs, as shown in Fig. 2. Besides consuming the largest amount of power, the RFPA wastes about 80-90% of the total power as heat dissipation, requiring air-conditioners, thus adding even more to the energy costs. As a result, the total efficiency of a conventional RFPA ranges from 5-20% only, depending on the semiconductor material and manufacturing process selection. The energy consumption also includes radiated power, but the radiated power per antenna decreases with an increase in the number of antennas [28]. Therefore, if highly efficient and linear RFPA may be used for each antenna, then the operational costs for the mobile network operators as well as the power consumption within the complete communication system can be optimized significantly [29].

DPD is a low-cost, and popular technique to compensate for RFPA's inherent nonlinearity and to make RFPA operating at relatively high efficiency, as shown in Fig.3. The input-output characteristics of an RFPA with nonlinearity is shown in Fig. 3(b), where p is input and y_{out} is output. If the DPD block can manipulate any incoming signal with appropriate inverse characteristic, as shown in Fig. 3(a), where x_{in} is input and p is the output, the final output y_{out} to the combination of DPD and RFPA is linear function of the original input signal x_{in}, as shown in Fig. 3(c). The combined effect of (DPD+RFPA) eliminates the inherent nonlinear behavior of the RFPA and establishes the concept of Green RFPA. The (DPD+RFPA) combination makes reliable and green HSR communications possible with linearity perspective, providing better user experience as well as with power efficiency perspective, providing less power waste [30].

The MIMO-DPD combination optimizes the energy consumption within the complete wireless communication system and ensures higher data throughputs. Furthermore, a Doherty RFPA is a promising architecture for DPD within HSR communication system to maintain optimal linearity-efficiency tradeoff [31]. The ultimate green reliable HSR communications can be achieved when DPD to Doherty power amplifiers is combined with MIMO transmission techniques.

IV. SYSTEM MODEL

Fig. 4 shows the green wireless practical MIMO communication model for intelligent HSR services. In this model, the BS is equipped with T antennas and serves a receiver having R antennas. The DPD block predistorts the original baseband signal in the digital domain, passes it through a digital-to-analog converter (DAC), then local oscillator (LO) and

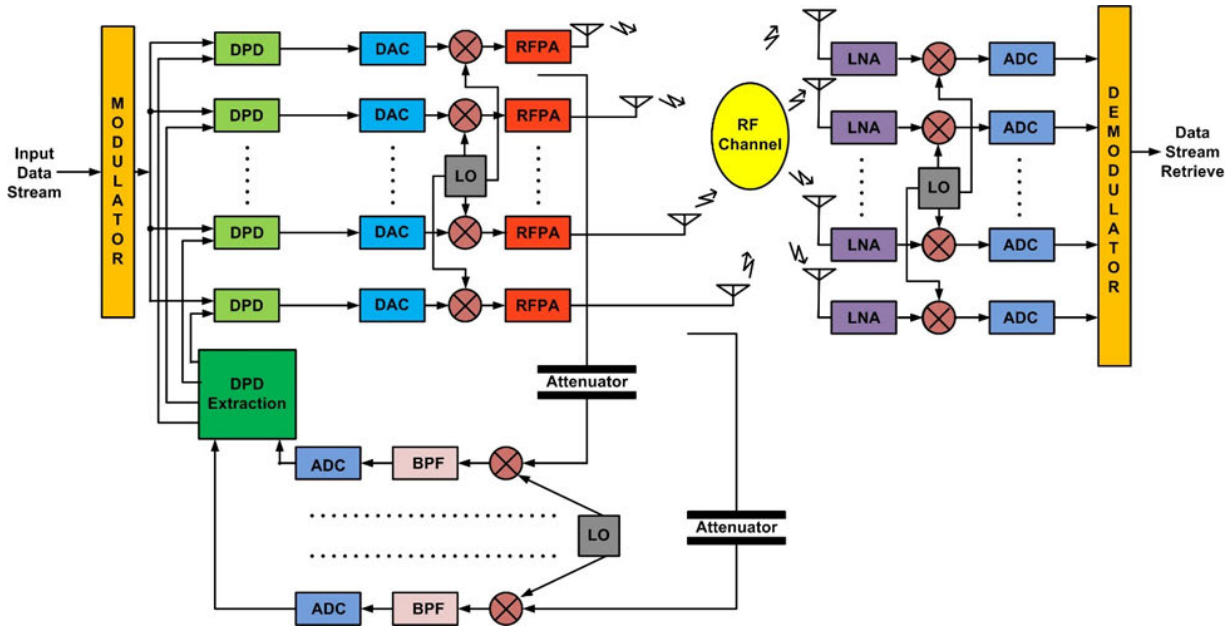

FIGURE 4. Green wireless practical MIMO communications system model.

mixer up-convert this signal to RF frequency. The RF signal is then fed through RFPA for transmitting more significant power to drive the transmitter antenna. DACs and analog-to-digital converters (ADCs) provide interfacing between the digital and analog components within the BS and the UE. The antenna transmits the signal on the RF channel. After its interception on the receiver side, LNA is used to amplify possibly weak signals. Finally, the demodulator achieves reconstruction of the signal.

Digital predistorters are used to compensate for the nonlinearity of RFPAs. The DPD parameters are extracted and updated by capturing and feeding the transmitted output signal via an attenuator, LO, bandpass filter, and an ADC. The comparison between the input and the captured output is made by DPD extraction unit that extracts the coefficients for the DPD block to carry out predistortion. The DPD block produces the predistortion function during the normal real-time communication system processing, while the DPD model extraction unit only invokes during the initial system setup or whenever there is a requirement to change the characteristics of HSR communication system.

A. END-TO-END MATHEMATICAL ANALYSIS

We have considered a MIMO communication system having T transmitting antennas and R receiving antennas. Each RF chain includes the following important blocks, which makes communication possible through the MIMO channel:

1) OFDM MODULATOR

The OFDM modulator performs inverse discrete Fourier Transform (IDFT) operation followed by cyclic prefix addition and parallel-to-serial conversion. The corresponding baseband equivalent expression of OFDM symbol with N subcarriers at the discrete time index n can be written as [32]

$$x_{in}^{t}[n] = \left\{ \begin{array}{ll} \frac{1}{n}\sum_{k=0}^{N-1} m_t(k) e^{j2\pi kn/N}, & -Ncy \le n \le N-1 \\ 0 & otherwise \end{array} \right\} \quad (1)$$

where $x_{in}^{t}[n]$ is the OFDM symbol input to the DPD of tth transmit antenna, $m_t(k)$ is the complex data symbol on kth subcarrier of the OFDM symbol, and N_{cy} is the cyclic prefix length. By the central limit theorem [33], if the number of subcarriers N is large, $m_t(k)$ can be assumed to be complex i.i.d. with zero mean and variance P_m and $x_{in}^{t}[n]$ to be a complex Gaussian process with zero mean and variance P_m/N.

2) DIGITAL PREDISTORTER

The input-output characteristics of DPD and RFPA shows that both have complementary characteristics. Thus, the output of a cascaded DPD+RFPA should ideally be a scaled replica of the original signal. The characteristics of DPD is usually modeled by nonlinear polynomial model, which can be expressed as [34], [35]

$$p^{t}[n] = \sum_{a=1}^{A} \alpha_a^t x_{in}^{t}[n] |x_{in}^{t}[n]|^{a-1} \quad (2)$$

where $p^{t}[n]$ is the DPD output at tth transmitting antenna when $x_{in}^{t}[n]$ is given as input. α_a^t are the complex nonlinearity coefficients of DPD for ath order nonlinearity, and A is the DPD nonlinearity order.

3) RFPA

The nonlinear characteristics of the RFPA can also be modeled by nonlinear polynomial model as

$$y_{out}^{t}[n] = \sum_{b=1}^{B} \sigma_{2b-1}^{t} p^{t}[n] |p^{t}[n]|^{2(b-1)} \quad (3)$$

where $p^t[n]$ and $y^t_{out}[n]$ are the input and output of the nonlinear RFPA of the tth transmitting antenna, respectively. B denotes the nonlinearity order and σ^t_{2b-1} are the complex nonlinearity coefficients of RFPA for *(2b-1)*th order nonlinearity.

4) CASCADED DPD+RFPA STRUCTURE

The signal is passed through the cascaded chain of DPD and RFPA. The coefficients of DPD in each RF chain are estimated separately depending upon the nonlinearity of the corresponding RFPA. From (2) and (3), the transmit signal at the tth transmit antenna can be represented as

$$y^t_{out}[n] = \sum_{b=1}^{B} \sigma^t_{2b-1} \left(\sum_{a=1}^{A} \alpha^t_a x^t_{in}[n] |x^t_{in}[n]|^{a-1} \right) \times \left(\left| \sum_{a=1}^{A} \alpha^t_a x^t_{in}[n] |x^t_{in}[n]|^{a-1} \right|^{2(b-1)} \right) \quad (4)$$

Rearranging, we get

$$y^t_{out}[n] = \sum_{c=1}^{A(2B-1)} \gamma^t_c x^t_{in}[n] |x^t_{in}[n]|^{c-1} \quad (5)$$

where γ^t_c are the complex nonlinear coefficients of the cascaded DPD+RFPA Green Communication system. The total number of coefficients required to realize the above equation is *A(2B-1)*. The γ^t_c coefficients for third-order nonlinear RFPA (*B=2*) and third-order nonlinear DPD (*A=3*) will be 9, and the expressions are given as follows:

$$\begin{aligned}
\gamma^t_1 &= \sigma^t_1 \alpha^t_1 \\
\gamma^t_2 &= \sigma^t_1 \alpha^t_2 \\
\gamma^t_3 &= \sigma^t_1 \alpha^t_3 + \sigma^t_3 \alpha^t_1 |\alpha^t_1|^2 \\
\gamma^t_4 &= \sigma^t_3 \alpha^t_1 U^t_{1,2} + \sigma^t_3 \alpha^t_2 |\alpha^t_1|^2 \\
\gamma^t_5 &= \sigma^t_3 \alpha^t_1 (|\alpha^t_2|^2 + U^t_{1,3}) + \sigma^t_3 \alpha^t_2 U^t_{1,2} + \sigma^t_3 \alpha^t_3 |\alpha^t_1|^2 \\
\gamma^t_6 &= \sigma^t_3 \alpha^t_1 U^t_{2,3} + \sigma^t_3 \alpha^t_2 (|\alpha^t_2|^2 + U^t_{1,3}) + \sigma^t_3 \alpha^t_3 U^t_{1,2} \\
\gamma^t_7 &= \sigma^t_3 \alpha^t_1 |\alpha^t_3|^2 + \sigma^t_3 \alpha^t_2 U^t_{2,3} + \sigma^t_3 \alpha^t_3 (|\alpha^t_2|^2 + U^t_{1,3}) \\
\gamma^t_8 &= \sigma^t_3 \alpha^t_2 |\alpha^t_3|^2 + \sigma^t_3 \alpha^t_3 U^t_{2,3} \\
\gamma^t_9 &= \sigma^t_3 \alpha^t_3 |\alpha^t_3|^2
\end{aligned}$$

where $U^t_{u,v} = \alpha^t_u \alpha^{t*}_v + \alpha^{t*}_u \alpha^t_v$.

The MIMO channel $\boldsymbol{H}[n]$ between transmitter and receiver is modeled with the impulse response method of the linear systems as [36]

$$\boldsymbol{H}[n] = \sum_{d=1}^{D} \boldsymbol{h}_d \delta[n-d] \quad (6)$$

where D is the number of received impulses that is equal to the total delay taps and $\boldsymbol{h}_d$ contains the MIMO channel coefficients for the dth multipath.

RECEIVED SIGNAL CHARACTERIZATION

The received signal vector at the MIMO-OFDM receiver is expressed as

$$\boldsymbol{m_o}[n] = \sum_{d=1}^{D} \boldsymbol{h}_d y^t_{out}[n-d] + \boldsymbol{w}[n] \quad (7)$$

where $\boldsymbol{m_o}[n]$ is an $R\times 1$ vector of received signals, $y_{out}[n]$ is a $T\times 1$ transmit signal vector at the DPD+RFPA cascaded output in transmitter and $\boldsymbol{w}[n]$ is an $R\times 1$ noise vector. Here $\boldsymbol{h}_d$ is given as

$$\boldsymbol{h}_d = \begin{bmatrix} h_d(1,1) & h_d(1,2) & \cdot & \cdot & h_d(1,T) \\ h_d(2,1) & h_d(2,2) & \cdot & \cdot & h_d(2,T) \\ \cdot & \cdot & \cdot & \cdot & \cdot \\ \cdot & \cdot & \cdot & \cdot & \cdot \\ h_d(R,1) & h_d(R,2) & \cdot & \cdot & h_d(R,T) \end{bmatrix} \quad (8)$$

where the MIMO channel coefficient $h_d(r,t)$ represents the complex delay amplitude of the dth delay tap between tth transmit antenna and rth receive antenna and is given as [37]

$$h_d(r,t) = Ad\, e^{j2\pi fcvn/c} \quad (9)$$

Here A_d is the complex gain associated with the dth multipath, f_c is the carrier frequency, v is the speed of train and c is the speed of light. It is to be noted that $\boldsymbol{h}_d$ is the response at delay d to an impulse at time n. It is assumed that $h_d(r,t)$ is a wide-sense stationary (WSS), f_s-limited complex Additive White Gaussian Noise (AWGN) process that is independent for different delay taps due to high mobility communication. Here f_s is the Doppler frequency, given as

$$fs = fc\frac{v}{c} \quad (10)$$

The received complex data symbol at the rth receive antenna, using (5), (7) and (8), can be written as

$$m_r[n] = \sum_{t=0}^{T-1} \sum_{d=0}^{D-1} h_d(r,t) \sum_{c=1}^{A(2B-1)} \gamma^t_c x^t_{in}[n-d] |x^t_{in}[n-d]|^{c-1} + w_r[n] \quad (11)$$

On removing the cyclic prefix and applying DFT operation, we get

$$m_r(k) = \sum_{n=0}^{N-1} m_r[n] e^{-j2\pi kn/N} \quad (12)$$

$$= \sum_{n=0}^{N-1} \sum_{t=0}^{T-1} \sum_{d=0}^{D-1} h_d(r,t) \sum_{c=1}^{A(2B-1)} \gamma^t_c x^t_{in}[n-d] |x^t_{in}[n-d]|^{c-1} \times e^{-j2\pi kn/N} + w_r(k) \quad (13)$$

where $w_r(k)$ is the AWGN in kth subcarrier at rth receive antenna. Using circular time shift property of DFT, the received complex data symbols at the kth subcarrier can be expressed as

$$m_r(k) = \sum_{t=0}^{T-1} \sum_{d=0}^{D-1} h_d(r,t) \sum_{n=0}^{N-1} \sum_{c=1}^{A(2B-1)} \gamma^t_c x^t_{in}[n] |x^t_{in}[n]|^{c-1}$$

$$\times e^{-j2\pi k(n+d)/N} + w_r(k) \tag{14}$$

$$= \sum_{t=0}^{T-1} \hat{h}_k(r,t)\, e_t(k) + w_r(k) \tag{15}$$

where $\hat{h}_k(r, t)$ is the effective channel coefficient from tth transmit antenna to rth receive antenna of kth subcarrier and can be written as [38]

$$\hat{h}_k(r,t) = \sum_{d=0}^{D-1} h_d(r,t)\, e^{-j2\pi kd/N} \tag{16}$$

and $e_t(k)$ is the effective nonlinear complex data symbol that can be written as

$$e_t(k) = \sum_{n=0}^{N-1} \sum_{c=1}^{A(2B-1)} \gamma_c^t x_{in}^t[n] |x_{in}^t[n]|^{c-1} \times e^{-j2\pi kn/N} \tag{17}$$

The R.H.S. of (17) can be canonically decomposed into multiplicative factor τ_t multiplied to the desired data symbol $m_t(k)$ and additive residual noise χ_t, thus

$$e_t(k) = \tau_t\, m_t(k) + \chi_t \tag{18}$$

where τ_t is the gain provided by the combination of DPD and RFPA. If τ_t is an unknown parameter, it can be written as [39]

$$E[e_t(k) m_t^*(k)] = \tau_t\, P_m \tag{19}$$

The variance $Var(\chi_t)$ of the residual noise can be given as

$$Var(\chi_t) = E[|\chi_t|^2] = E[|e_t(k)|^2] - P_m |\tau_t|^2 \tag{20}$$

Using (15) and (18), the received complex data symbol $m_r(k)$ can be expressed as

$$m_r(k) = \sum_{t=0}^{T-1} \hat{h}_k(r,t)\{\tau_t\, m_t(k) + \chi_t\} + w_r(k) \tag{21}$$

Using channel equalization technique [40], the complex data symbol on kth subcarrier of the OFDM symbol associated with tth transmit antenna in the MIMO channel is best approximated as

$$\hat{m}_t(k) = \tau_t m_t(k) + \chi_t + [(\hat{\boldsymbol{H}}(k))^{\dagger} w(k)]^t \tag{22}$$

where $[(\hat{\boldsymbol{H}}(k))^t w(k)]^t$ is the tth element of vector $(\hat{\boldsymbol{H}}(k))^t w(k)$, $\hat{\boldsymbol{H}}(k)$ is the $R \times T$ MIMO channel at the kth subcarrier after channel equalization operation whose elements are $\hat{h}_k(r,t)$ and $\boldsymbol{w}(k)$ is the $R \times 1$ AWGN vector whose elements are $w_r(k)$.

Thus, the resultant SNR for the kth subcarrier is given as

$$\rho_t(k) = \frac{P_m |\tau_t|^2}{Var(\chi_t) + [((H_k)^H H_k)^{-1}]^t N_0} \tag{23}$$

or

$$\rho_t(k) = \frac{\rho_m}{Var(\chi_t)/N_0 + \frac{1}{\psi_k}} |\tau_t|^2 \tag{24}$$

where $\rho_m = \frac{P_m}{N_0}$ is the received SNR in the static channel, and $\psi_k = \frac{1}{[((H_k)^H H_k)^{-1}]^t}$ has a Chi-squared distribution with $2(R\text{-}T+1)$ degrees of freedom [41].

Hence the average SNR across all the transmitting branches and all the subcarriers can be evaluated as

$$\rho_{av} = \frac{1}{TN} \sum_{t=1}^{T} \sum_{k=1}^{N} \rho_t(k) \tag{25}$$

The BLER and throughput are the key performance indicators to study the impact of MIMO schemes in any modern high-speed communication system [42]–[44]. The BLER value establishes the reliability of data transmission over an HSR communication system. The data transmission is reliable if it efficaciously decodes the transport block, which means that the cyclic redundancy check (CRC) of the transport block should be checked and appropriately matched with the receiver CRC. BLER is measured after channel decoding, and de-interleaving has been done after performing the CRC for all transport blocks. Larger values of BLER indicate a bad RF environment that again can cause low downlink throughput. BLER is represented by Bl and is calculated as

$$Bl = \frac{\sum_{SU\ Start}^{SU\ Stop} (1 - CRC\ Check)}{\sum_{SU\ Start}^{SU\ Stop} (1)} \tag{26}$$

where SU is the abbreviation of subframe and CRC Parity indicates the *CRC Check* result for each subframe. The *CRC Check* value '1' means CRC Check is successful and '0' means CRC Check fails. The receiver is assumed to have a latency of one subframe, i.e., one millisecond duration, which shows that the throughput calculation should atleast start after the first subframe, i.e., $SU\ Start \geq 1$.

The CRC failure criteria for indicating out-of-synchronization is taken so that the downlink connection has to fail atleast 200 milliseconds before being lost. Moreover, at least 20 consecutive lost frames are needed to ensure the out-of-synchronization state. However, as soon as the links get better and one CRC is received correctly, the links are considered to be in-synchronization again.

A modern wireless communication receiver with error detection and correction capability is modeled as [45]

$$Bl_m = \left\{ \begin{matrix} 1, & \rho_m < \rho_{th} \\ 0, & \rho_m > \rho_{th} \end{matrix} \right\} \tag{27}$$

where Bl_m represents the BLER of a pure Line of Sight (LoS) channel and ρ_{th} is the threshold level of the received signal power. Any connected UE on a high-speed train experiences the radio link quality in terms of BLER values with respect to SNR levels. Thus the conception of deteriorating radio link condition for the HSR communications also corresponds to the observed BLER value. If this value exceeds the threshold level of 0.1, it signifies that eNodeB and UE are not synchronized to provide reliable communications [46].

As BLER changes with time due to time-varying fading in a dynamic channel, it must be averaged for this case. The average BLER value Bl_{av} in a fading channel is a function of average SNR ρ_{av}. The static LOS BLER Bl_m and the average BLER Bl_{av} are related as

$$Bl_{av} = \int_0^{\infty} Bl_m f(\rho_m; \rho_{av})\, d\rho_m \tag{28}$$

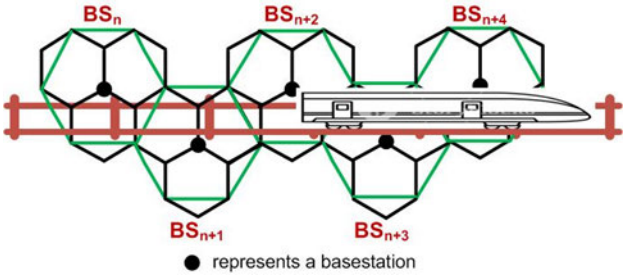

FIGURE 5. Infrastructure-to-train scenario.

where $f(\rho_m; \rho_{av})$ is the probability density function (PDF) of the fading power level ρ_m.

Substituting (26) into (27), we get

$$Bl_{av} = \int_0^{\rho_{th}} f(\rho_m; \rho_{av})\, d\rho_m \tag{29}$$

The throughput data rate of MIMO communication system for dealing with error correction codes is expressed as [47]

$$\Gamma = \frac{\Gamma \max}{T} \sum_{t=1}^{T} (1 - Bl) \tag{30}$$

where Γ_{max} is the maximum throughput achieved at high SNR. This equation is valid for static LOS MIMO channel (Bl_m exists with ρ_m) and dynamic fading MIMO environments (Bl_{av} exists with ρ_{av}).

B. ARRANGEMENTS AND ASSUMPTIONS

The main goal with HSR communications is to achieve various high data rate applications for train operators and passengers. The train services are implemented in two imperative railway transportation scenarios – (1) during travelling, known as infrastructure-to-train scenario, and (2) when the user is within the railway station platform range, either inside or outside the train, known as an inside-station scenario. The infrastructures are real-time connected and interactive, supported by high data rate bidirectional data streams with low latencies.

In the infrastructure-to-train scenario, no specific topographical details are taken into account. BSs are placed in a regular grid, having a hexagonal layout using the clover-leaf cell configuration scheme, which has been widely used in cellular communications. The cells are configured in three ways in this scheme: single-cell, 1-tier, or 2-tier configuration [48], [49]. Each BS has three sectors fed by an antenna, and the BSs are placed on the lattice of the new bigger hexagon. We took a single cell clover-leaf hexagonal layout with three cells per site, as shown in Fig. 5, for the simulation arrangement. Users are distributed uniformly over the whole area.

As a wireless communication environment grows uneven traffic load, i.e., inside-station scenario, it will be converted into "hotspot" cells. These cells are considered to have a substantially higher traffic load than the designated load. The authors took the scenario of a railway station platform with

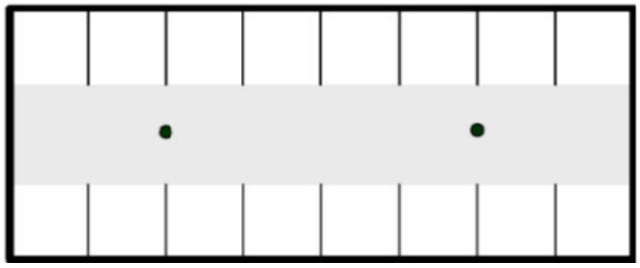

FIGURE 6. Inside-station scenario.

TABLE 2. System model parameters.

Parameters	Value(s)
Transmission System	LTE-R, Downlink
Channel Type	Outdoor LoS, Indoor LoS
Traffic Type	Full Buffer Model
Sampling Frequency	15.36 MHz
Channel Bandwidth	10 MHz
Carrier Frequency	2 GHz
Diversity Mode	Full, Transmit
Antenna Configuration	SISO, MIMO
Frame Mode	FDD
FFT Size	1024
Radio Frames	200 (in numbers)
Subframes	2000 (in numbers)
Radio Frame Duration	10 ms
Coding Scheme	FEC Turbo Coding, Rate = 1/6
Mapping Type	64-QAM
Resource Block	12 tones over 1 ms
Subcarrier Spacing	15 kHz
Channel Estimation Scheme	Minimum Mean Square Error
MIMO Detection Scheme	Maximum Likelihood Detection
RFPA Type	Doherty

dimensions 120 m x 50 m. Let us suppose that the height of the roof is 6 m and the inside-station structure contains 16 sheds/rooms of 15 m x 15 m. The BSs are placed within the open space in front of the sheds/rooms at 30 m and 90 m, as shown in Fig. 6, with respect to the left side of the structure.

This paper focuses on efficient communication for high-speed trains. The end-to-end communication system analysis, considering the presence of practical nonlinear RFPAs for high-speed communications, has been reported for the first time in terms of packet loss / BLER and throughput. The study does not depend only on cell configuration, but we have provisioned other parameters like sampling frequency, carrier frequency, channel bandwidth, multiple antenna configurations, complex modulation mapping scheme, channel estimation technique, detection technique, multiple speed scenarios, BS antenna height, BS antenna gain, the inter-site distance, the minimum distance between UE in the train and the serving cell.

These system model parameters are assigned real values during the simulation stage, as given in Table 2 and Table 3. It is to be noted that the parameters shown in Table 2 have the same values in infrastructure-to-train and inside-station scenarios. In contrast, Table 3 notifies those parameters that have different values for the two cases. The acceptable range of SNR values starts from 15 dB for successful data transmission in all modern wireless communication technologies,

TABLE 3. System model parameters.

Parameters	Value(s)	
	inside-station	infrastructure-to-train
Speeds of interest	0-3 kmph	0-200 kmph
Inter-site Distance	60 m	1732 m
BS Antenna Height	6 m	35 m
BS Antenna Gain	0 dBi	17 dBi
Minimum Distance between UE and the serving cell	3 m	35 m

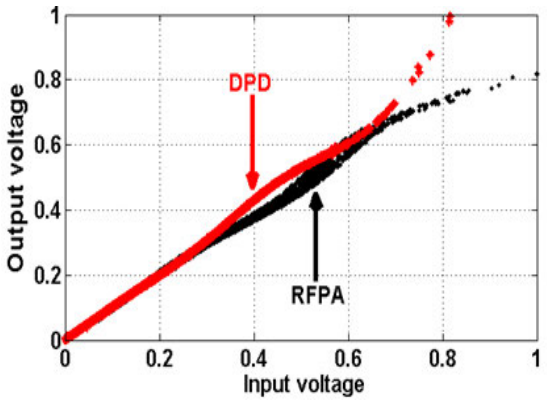

FIGURE 7. DPD and RFPA results in terms of input and output voltage.

including LTE. In contrast, the SNR values from 15-25 dB represent low signal strength, from 25-40 dB represent good signal strength, and the SNR values over 40 dB provide excellent signal strength [50]. Doherty PAs are utilized at transmitters.

V. RESULTS AND DISCUSSION

In this section, the results are presented to evaluate the end-to-end performance of the practical HSR communication system. The analysis is carried out with DPD and without DPD in terms of BLER and throughput with respect to SNR. Fig. 7 shows the DPD results for achieving linearization in terms of normalized input and output voltages, where the scattering in the outputs is observed due to the channel effect. Fig. 8 shows the measured ACPR, average output power, and corresponding power added efficiency (PAE) without DPD and with DPD compensation. The ACPR denotes the adjacent channel interference and is given as the ratio of the main channel power to the power in the adjacent channels.

The authors use -45 dBc as a threshold value to the acceptable ACPR performance for achieving perfect linearization. The achieved average output power without DPD arrangement, at this threshold $\simeq -45$ dBc, is 15.28 dBm, whereas it is 18.36 dBm with DPD. The PAE increases from 6.66% to 13.28% at the threshold ACPR $\simeq -45$ dBc. Fig. 7 and Fig. 8 establish that the communication systems become power-efficient after DPD inclusion. Therefore, the DPD technique may be helpful in achieving the objective of Green HSR communications.

With the proposed DPD and RFPA for each transmitter branch, the infrastructure-to-train scenario is represented in Figs. 9, 10, 11, 12, 13, and 14, and the inside-station

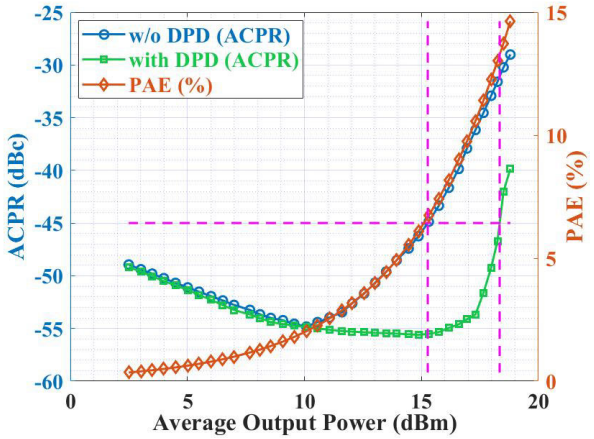

FIGURE 8. Measured ACPR, measured output power and PAE for LTE signal.

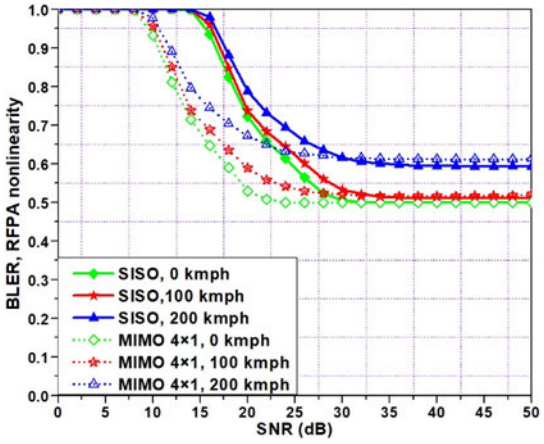

FIGURE 9. BLER without DPD at various train speeds for SISO and MIMO configurations.

scenario is represented in Figs. 15 and 16. The investigations are done for SISO and several MIMO antenna configurations, for train speeds varying from 0-200 kilometers per hour (kmph), and for pedestrian speeds ranging from 0-3 kmph.

The graphical representations in the figures with the caption 'RFPA' denote characteristics having RFPA nonlinearity; and the caption 'Green' indicates the characteristics, where RFPA nonlinearity is compensated with DPD. The caption 'stationary' represents the train speed of 0 kmph and 'high speed' represents the train speed equals to 200 kmph in all graphs corresponding to the infrastructure-to-train scenario. On the contrary, the caption 'stationary' represents the pedestrian speed of 0 kmph and 'high speed' represents the pedestrian speed of 3 kmph corresponding to the inside-station scenario graphs.

The authors comprise a three-way analysis for the infrastructure-to-train scenario. Figs. 9 and 10 cover the effect of mobility on various antenna configurations with RFPA nonlinearity. Figs. 11 and 12 show the linearization effect on various mobilities for MIMO 4×1 configuration. Figs. 13 and 14 analyze different MIMO configurations, including several transmit and receive diversity cases, with the DPD arrangement at high mobility. Figs. 15 and 16 show the same aforesaid analysis for the inside-station scenario.

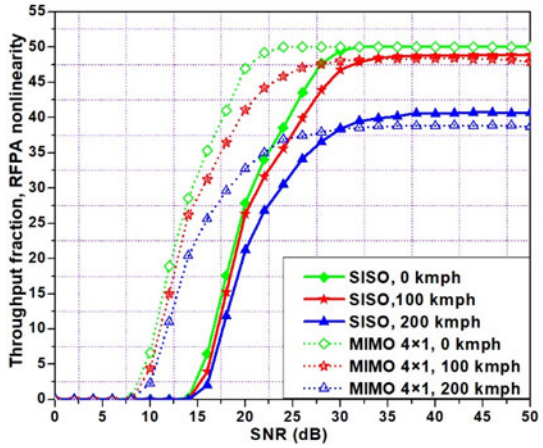

FIGURE 10. Throughput without DPD at various train speeds for SISO and MIMO configurations.

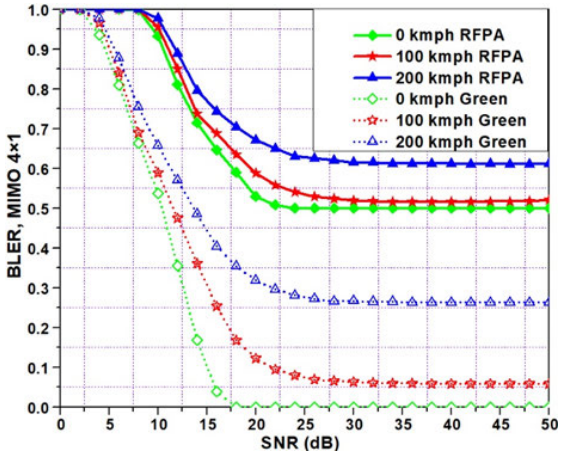

FIGURE 11. BLER with DPD and without DPD at different train speeds for MIMO 4 × 1 configuration. Here 'Green' refers to the case when RFPA nonlinearity is compensated using the DPD technique.

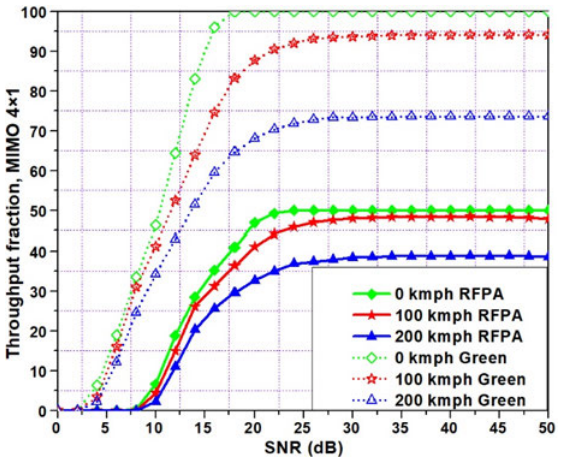

FIGURE 12. Throughput with DPD and without DPD at different train speeds for MIMO 4 × 1 configuration. Here 'Green' refers to the case when RFPA nonlinearity is compensated using the DPD technique.

Figs. 9 and 10 represent the cases when no predistortion is done to linearize the RFPA. The figures clearly show that RFPA nonlinearity deteriorates the BLER and throughput performances. It is seen that without DPD, more than 50 % of blocks are erroneously received to the total data blocks transmitted over the RF channel. The BLER and throughput performances degrade further with increasing train speeds. Both of these parameters have comparatively better results at low SNR values for higher order MIMO configurations. In contrast, SISO configuration gives comparatively better results at high SNR values. The best BLER value achieved in this case, as in Fig. 9, is 0.5 for which at least an SNR of 22 dB is needed, which is achieved with MIMO 4 × 1 configuration at 0 kmph. The SISO configuration requires at least 32 dB SNR to have the same BLER. However, if SNR requirement is fixed at 22 dB, from Fig. 10, the achieved maximum throughput without DPD is only 50 % for MIMO 4 × 1 configuration at 0 kmph. With SISO configuration, the system without DPD achieves maximum throughput equals to 4.57 Mbps at 0 kmph speed and 3.73Mbps at 200 kmph. The maximum throughput achieved with MIMO 4 × 1 without compensating RFPA nonlinearity for 0 kmph and 200 kmph is 4.12 Mbps and 3.19 Mbps, respectively only. The results also establish that no antenna configuration can attain the required BLER value of 0.1 for successful data transmission due to RFPA nonlinearity. It envisages that more power is required to make data transmission with nonlinear RFPAs, but the achieved throughput is still less.

Figs. 11 and 12 represent the results for MIMO 4 × 1 with and without DPD at different train speeds. If BLER value is taken as 0.1 (equivalent to 10 % of the maximum) in Fig. 11, a minimum SNR value of 15 dB is needed to reach this target BLER. This has been achieved with MIMO 4 × 1 at 0 kmph with DPD arrangement, whereas the target BLER has never been achieved with the systems having RFPA nonlinearity. The same target BLER is achieved at an SNR of 22 dB with MIMO-DPD 4 × 1 configuration when the train is running at 100 kmph. This implies that the signal needs high power to get transmitted at high mobilities. The signal may need even more power if the nonlinearity is not compensated earlier. From Fig. 12, the throughput to achieve the required 0.1 BLER value is 95 % with MIMO 4 × 1 configuration at 0 kmph for 15 dB SNR with DPD and 90 % with MIMO 4 × 1 configuration at 100 kmph for 22 dB SNR with DPD. However, if the required SNR is 15 dB for MIMO 4 × 1 configuration, from Fig. 12, the maximum throughput values with DPD are 95 %, 75 %, and 60 % at train speeds 0 kmph, 100 kmph, and 200 kmph, respectively. On the contrary, if the RFPA nonlinearity is not mitigated, the throughput degrades to 35 %, 30 %, and 25 % at the same 15 dB SNR for train speeds 0 kmph, 100 kmph, and 200 kmph, respectively.

Figs. 13 and 14 represent the results with DPD for the trains at a high speed of 200 kmph. The results are taken for SISO and several other MIMO configurations. If BLER value is limited at 0.1 in Fig. 13, the SNR values equal to 22 dB and 24 dB are needed to reach this target BLER with DPD-MIMO 1 × 8, and DPD-MIMO 8 × 8 communication systems. It is to be noted that DPD-MIMO 4 × 4, DPD-MIMO 2 × 2, DPD-MIMO 8 × 1, and DPD-SISO communication systems are not able to achieve this target

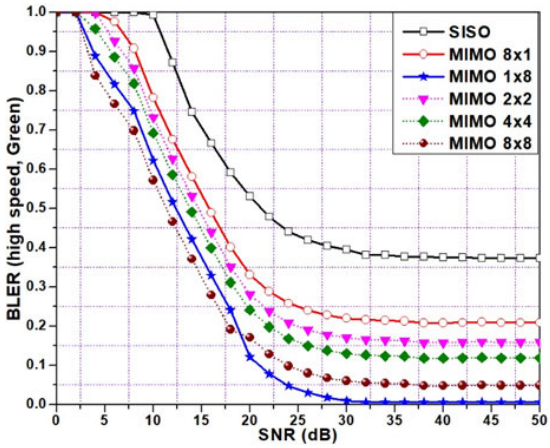

FIGURE 13. BLER with DPD for SISO and MIMO configurations for high speed train. Here 'Green' refers to the case when RFPA nonlinearity is compensated using the DPD technique.

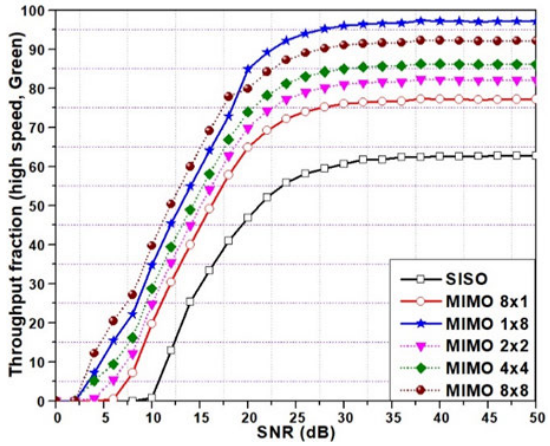

FIGURE 14. Throughput with DPD for SISO and MIMO configurations for high speed train. Here 'Green' refers to the case when RFPA nonlinearity is compensated using the DPD technique.

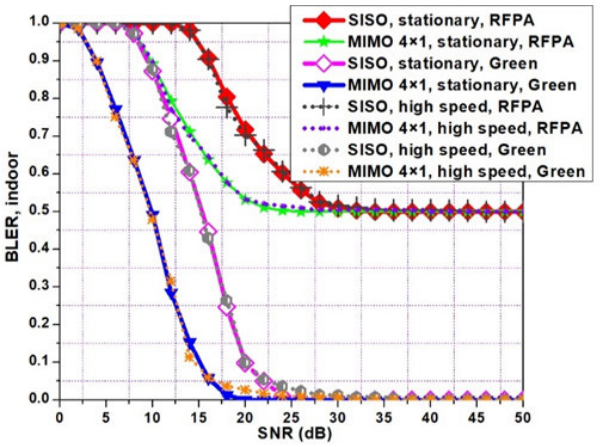

FIGURE 15. BLER with DPD for the inside-station scenario. Here 'Green' refers to the case when RFPA nonlinearity is compensated using the DPD technique.

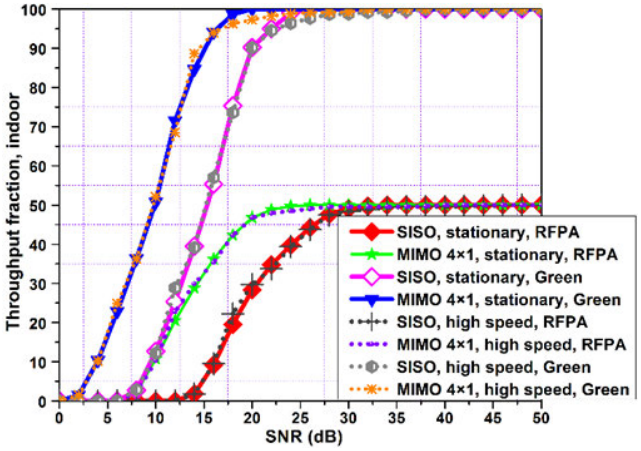

FIGURE 16. Throughput with DPD for the inside-station scenario. Here 'Green' refers to the case when RFPA nonlinearity is compensated using the DPD technique.

BLER of 0.1 at 200 kmph and, thus, are not able to provide reliable communications for very high-speed trains. It means that 8×8 and 1×8 DPD-MIMO modes offer least signal power requirement. It is also envisaged that DPD-MIMO 8×8 delivers better results for SNR values less than 20 dB; but for SNR values greater than 20 dB, the DPD-MIMO 1×8 mode offers the best results. At the same time, from Fig. 14, the same configuration achieves 90 % throughput at 0.1 BLER value. The maximum throughput achieved is 92.25 % at high mobility of 200 kmph with DPD-MIMO 1×8 configuration for SNR 30 dB. It reveals that LTE-R performs successful data transmission with DPD for even low strength signals, but this may be the case when train speed is less than 200 kmph. The power required to drive RFPAs for reliable broadband HSR communication at higher speeds is more, even with DPD. While the maximum throughput achieved for high-speed train with DPD for SISO configuration is only 5.74 Mbps, it is 8.85 Mbps for MIMO 1×8 configuration to the same conditions for SNR values greater than 40 dB.

The DPD improves BLER and throughput performances for the inside-station scenario. It is evident from Fig. 15 and Fig. 16 that the MIMO diversity mode 4×1 gives the best throughput value with low power requirement and achieves the acceptable BLER value. If the SNR value is kept fixed at 15 dB and DPD is done for high speed inside-station scenario, the throughput reaches from 9.5 % of its maximum value to 57 % with SISO and from 35.35 % to 93.95 % with MIMO 4×1 configuration. Furthermore, the acceptable BLER value 0.1 for reliable data transmission is achieved for MIMO 4×1 configuration with the same SNR at both 0 kmph and 3 kmph with DPD, while has been unacceptable without DPD.

The throughput values for infrastructure-to-train scenario for the high speed (200 kmph) case without and with DPD at 40 dB SNR are given in Table 4. The throughput values for the inside-station scenario for stationary (0 kmph) and high speed (3 kmph) cases without and with DPD at 15 dB SNR are given in Table 5.

It is seen that video represents the greatest data usage by passengers during journeys, where most of the video applications adapt their streaming rates utilizing the available bandwidth and, therefore, they may continue to operate even if throughput rates drop. The error in receiving data packets during video transmission in very high-speed trains, may affect the quality, but it does not entirely discard the

TABLE 4. Throughput (Mbps): infrastructure-to-train scenario.

infrastructure-to-train case	Antenna Configuration	Without DPD	With DPD
High speed	SISO	2.12	5.70
	MIMO 8×1	2.58	7.06
	MIMO 1×8	4.15	8.80
	MIMO 2×2	2.91	6.76
	MIMO 4×4	3.39	7.14
	MIMO 8×8	3.78	7.89

TABLE 5. Throughput (Mbps): inside-station scenario.

inside-station cases	Antenna Configuration	Without DPD	With DPD
Stationary	SISO	0.84	5.06
	MIMO 2×1	2.32	7.29
	MIMO 4×1	2.99	7.77
High speed	SISO	0.87	5.21
	MIMO 2×1	2.42	7.37
	MIMO 4×1	2.92	7.75

transmitted information. The BLER and throughput performances can further be improved, particularly for video transmissions, by increasing the number of retransmission processes.

VI. CONCLUSION

The RFPA nonlinearity compensation using DPD for green HSR communications is analyzed. It is realized that ITS services enhance the safety and convenience of both train operators and train passengers. The analysis is done for the infrastructure-to-train and inside-station scenarios with and without DPD arrangement. The BLER and data throughput performance metrics are evaluated for the emerging 10 MHz LTE-R communications system with SISO and MIMO modes in terms of SNR for 64QAM downlink mapping at various train speeds upto 200 kmph and various pedestrian speeds upto 3 kmph. It is investigated that the recommended LTE-R specifications with MIMO-DPD result in a higher BLER due to the fast fading channel effect, and the radio link establishment procedures need more time for radio access with increasing speeds.

While analyzing the behavior of a modern practical communications system, RFPA should never be assumed linear. The paper establishes that RFPA nonlinearity deteriorates the BLER and throughput performances, and that, without DPD, more than 50 % blocks are received with errors to the total data blocks transmitted over the RF channel. The BLER and throughput performances degrade further with increasing train speeds. It implies that more transmission power is needed to send signals at high mobility. The additional signal power is to be given if nonlinearity is not compensated earlier. It is also revealed that LTE-R achieves successful data transmission with DPD for even low strength signals. The power requirement to drive RFPAs for reliable broadband HSR communications at higher speeds is more, even with DPD. The paper further establishes that the DPD technique, when combined with MIMO schemes, gives optimal results and is the ultimate approach to achieve reliable Green HSR communications.

In this paper, we also analyzed the joint nonlinear behaviors of RFPA and DPD for the HSR MIMO communications system. An end-to-end analytical methodology is developed using mathematical expressions to obtain the closed-form expressions of BLER and throughput. A communication engineer may easily utilize the analysis to design the link budget for high-speed MIMO wireless communication systems with the help of a realistic power consumption model. The framework can be employed for complex modulation mapping schemes like 128-QAM or 256-QAM to achieve higher throughput rates. The proposed analysis can also be extended to the flexible and heterogeneous cell structures, which will be a subject of our future work.

REFERENCES

[1] *World Urbanization Prospects: The 2018 Revision (ST/ESA/SER.A/420)*, United Nations, Department of Economic and Social Affairs, Population Division. New York, NY, USA, 2019.

[2] *Smart Sustainable Cities: An Analysis of Definitions*, document FGSSC-10/2014, ITU, ITU-T Focus Group on Smart Sustainable Cities, Oct. 2014, pp. 1–73.

[3] C. Facanha, K. Blumberg, and J. Miller, *Global Transportation Energy and Climate Roadmap*. Washington DC, USA: The International Council on Clean Transportation, Nov. 2012, pp. 1–109.

[4] J. Moreno, L. de Haro, C. Rodriguez, L. Cuellar, and J. M. Riera, "Keyhole estimation of an MIMO-OFDM train-to-wayside communication system on subway tunnels," *IEEE Antennas Wireless Propag. Lett.*, vol. 14, pp. 88–91, 2015.

[5] J. Yang, B. Ai, S. Salous, K. Guan, D. He, G. Shi, and Z. Zhong, "An efficient MIMO channel model for LTE-R network in high-speed train environment," *IEEE Trans. Veh. Technol.*, vol. 68, no. 4, pp. 3189–3200, Apr. 2019.

[6] T. Zhou, C. Tao, S. Salous, and L. Liu, "Measurements and analysis of angular characteristics and spatial correlation for high-speed railway channels," *IEEE Trans. Intell. Transp. Syst.*, vol. 19, no. 2, pp. 357–367, Feb. 2018.

[7] L. M. Correia, D. Zeller, O. Blume, D. Ferling, Y. Jading, I. Gódor, G. Auer, and L. V. D. Perre, "Challenges and enabling technologies for energy aware mobile radio networks," *IEEE Commun. Mag.*, vol. 48, no. 11, pp. 66–72, Nov. 2010.

[8] D. Kong, S. Hu, Y. Wu, J. Wang, C. Xiong, Q. Yu, Z. Shi, Z. Liu, T. Chen, Y. Yin, S. Hosaka, and Y. Liu, "Realization of a power-efficient transmitter based on integrated artificial neural network," *IEEE Access*, vol. 6, pp. 68773–68781, Nov. 2018.

[9] J. Joung, C. K. Ho, K. Adachi, and S. Sun, "A survey on power-amplifier-centric techniques for spectrum- and energy-efficient wireless communications," *IEEE Commun. Surveys Tuts.*, vol. 17, no. 1, pp. 315–333, 1st Quart., 2015.

[10] M. Younes, A. Kwan, M. Rawat, and F. M. Ghannouchi, "Three-dimensional digital predistorter for concurrent tri-band power amplifier linearization," in *IEEE MTT-S Int. Microw. Symp. Dig.*, Jun. 2013, pp. 1–4.

[11] J. Kim, P. Roblin, D. Chaillot, and Z. Xie, "A generalized architecture for the Frequency- selective digital predistortion linearization technique," *IEEE Trans. Microw. Theory Techn.*, vol. 61, no. 1, pp. 596–605, Jan. 2013.

[12] A. Abdelhafiz, L. Behjat, F. M. Ghannouchi, M. Helaoui, and O. Hammi, "A high-performance complexity reduced behavioral model and digital predistorter for MIMO systems with crosstalk," *IEEE Trans. Commun.*, vol. 64, no. 5, pp. 1996–2004, May 2016.

[13] J. A. Galaviz-Aguilar, C. Vargas-Rosales, and E. Tlelo-Cuautle, "RF-PA modeling of PAPR: A precomputed approach to reinforce spectral efficiency," *IEEE Access*, vol. 8, pp. 138217–138235, 2020.

[14] O. Hammi and F. M. Ghannouchi, "Twin nonlinear two-box models for power amplifiers and transmitters exhibiting memory effects with application to digital predistortion," *IEEE Microw. Compon. Lett.*, vol. 19, no. 8, pp. 530–532, Aug. 2009.

[15] Y. Liu, C. Huang, X. Quan, P. Roblin, W. Pan, and Y. Tang, "Novel linearization architecture with limited ADC dynamic range for green power amplifiers," *IEEE J. Sel. Areas Commun.*, vol. 34, no. 12, pp. 3902–3914, Dec. 2016.

[16] P. Jaraut, M. Rawat, and F. M. Ghannouchi, "Composite neural network digital predistortion model for joint mitigation of crosstalk, I/Q imbalance, nonlinearity in MIMO transmitters," *IEEE Trans. Microw. Theory Techn.*, vol. 66, no. 11, pp. 5011–5020, Nov. 2018.
[17] P. M. Suryasarman and A. Springer, "A comparative analysis of adaptive digital predistortion algorithms for multiple antenna transmitters," *IEEE Trans. Circuits Syst. I, Reg. Papers*, vol. 62, no. 5, pp. 1412–1420, May 2015.
[18] M. Rawat, P. Roblin, C. Quindroit, K. Salam, and C. Xie, "Concurrent dual-band modeling and digital predistortion in the presence of unfilterable harmonic signal interference," *IEEE Trans. Microw. Theory Techn.*, vol. 63, no. 2, pp. 625–637, Feb. 2015.
[19] M. Rawat, K. Rawat, and F. M. Ghannouchi, "Three-layered biased memory polynomial for dynamic modeling and predistortion of transmitters with memory," *IEEE Trans. Circuits Syst. I, Reg. Papers*, vol. 60, no. 3, pp. 768–777, Mar. 2013.
[20] Y. Zhou, K. C. Dey, M. Chowdhury, and K. Wang, "Process for evaluating the data transfer performance of wireless traffic sensors for real-time intelligent transportation systems applications," *IET Intell. Transp. Syst.*, vol. 11, no. 1, pp. 18–27, Feb. 2017.
[21] L. Zhu, F. R. Yu, B. Ning, and T. Tang, "Handoff performance improvements in MIMO-enabled communication-based train control systems," *IEEE Trans. Intell. Transp. Syst.*, vol. 13, no. 2, pp. 582–593, Jun. 2012.
[22] J. Zhao, Y. Liu, C. Wang, L. Xiong, and L. Fan, "High-speed based adaptive beamforming handover scheme in LTE-R," *IET Commun.*, vol. 12, no. 10, pp. 1215–1222, 2018.
[23] S. Marcus, G. Gach, and B. Wyler, "Study on the architecture of on-board radio communication equipment," Eur. Union Agency Railways, Paris, France, Tech. Rep. FR01T17J09_ERA_OP31_RP, Sep. 2018, pp. 1–178, vol. 8.
[24] H. Cho, S. Shin, G. Lim, C. Lee, and J.-M. Chung, "LTE-R handover point control scheme for high-speed railways," *IEEE Wireless Commun.*, vol. 24, no. 6, pp. 112–119, Dec. 2017.
[25] R. He, B. Ai, G. Wang, K. Guan, Z. Zhong, A. F. Molisch, C. Briso-Rodriguez, and C. P. Oestges, "High-speed railway communications: From GSM-R to LTE-R," *IEEE Veh. Technol. Mag.*, vol. 11, no. 3, pp. 49–58, Sep. 2016.
[26] M. Liem and V. B. Mendiratta, "Mission critical communication networks for railways," *Bell Labs Tech. J.*, vol. 16, no. 3, pp. 29–46, Dec. 2011.
[27] S. Cui, A. J. Goldsmith, and A. Bahai, "Energy-efficiency of MIMO and cooperative MIMO techniques in sensor networks," *IEEE J. Sel. Areas Commun.*, vol. 22, no. 6, pp. 1089–1098, Aug. 2004.
[28] T. L. Marzetta, "Noncooperative cellular wireless with unlimited numbers of base station antennas," *IEEE Trans. Wireless Commun.*, vol. 9, no. 11, pp. 3590–3600, Nov. 2010.
[29] Z. Hasan, H. Boostanimehr, and V. K. Bhargava, "Green cellular networks: A survey, some research issues and challenges," *IEEE Commun. Surveys Tuts.*, vol. 13, no. 4, pp. 524–540, 4th Quart., 2011.
[30] L. Guan and A. Zhu, "Green communications: Digital predistortion for wideband RF power amplifiers," *IEEE Microw. Mag.*, vol. 15, no. 7, pp. 84–99, Nov./Dec. 2014.
[31] W. C. E. Neo, J. Qureshi, M. J. Pelk, J. R. Gajadharsing, and L. C. N. de Vreede, "A mixed-signal approach towards linear and efficient N-way Doherty amplifiers," *IEEE Trans. Microw. Theory Techn.*, vol. 55, no. 5, pp. 866–879, May 2007.
[32] H. Hemesi, A. Abdipour, and A. Mohammadi, "Analytical modeling of MIMO-OFDM system in the presence of nonlinear power amplifier with memory," *IEEE Trans. Commun.*, vol. 61, no. 1, pp. 155–163, Nov. 2013.
[33] A. Papoulis and S. U. Pillai, *Probability, Random Variables and Stochastic Processes*, 4th ed. New York, NY, USA: McGraw-Hill, 2002.
[34] P. Aggarwal and V. A. Bohara, "On the multiband carrier aggregated nonlinear LTE-A system," *IEEE Access*, vol. 5, pp. 16930–16943, 2017.
[35] P. Aggarwal and V. A. Bohara, "A nonlinear downlink multiuser MIMO-OFDM systems," *IEEE Wireless Commun. Lett.*, vol. 6, no. 3, pp. 414–417, Jun. 2017.
[36] Y. Li, "Pilot-symbol-aided channel estimation for OFDM in wireless systems," *IEEE Trans. Veh. Technol.*, vol. 49, no. 4, pp. 1207–1215, Jul. 2000.
[37] T. R. Dean, M. Chowdhury, N. Grimwood, and A. J. Goldsmith, "Rethinking modulation and detection for high Doppler channels," *IEEE Trans. Wireless Commun.*, vol. 19, no. 6, pp. 3629–3642, Jun. 2020.
[38] A. Goldsmith, *Wireless Communications*, 1st ed. New York, NY, USA: Cambridge Univ. Press, 2005.
[39] P. Aggarwal and V. A. Bohara, "Analytical characterization of dual-band multi-user MIMO-OFDM system with nonlinear transmitter constraints," *IEEE Trans. Commun.*, vol. 66, no. 10, pp. 4536–4549, Oct. 2018.
[40] G. Amarasuriya, C. Tellambura, and M. Ardakani, "Multi-way MIMO amplify-and-forward relay networks with zero-forcing transmission," *IEEE Trans. Commun.*, vol. 61, no. 12, pp. 4847–4863, Dec. 2013.
[41] D. Morales-Jimenez, J. F. Paris, J. T. Entrambasaguas, and K.-K. Wong, "On the diagonal distribution of a complex wishart matrix and its application to the analysis of MIMO systems," *IEEE Trans. Commun.*, vol. 59, no. 12, pp. 3475–3484, Dec. 2011.
[42] T. Cui, F. Lu, V. Sethuraman, A. Goteti, S. P. N. Rao, and P. Subrahmanya, "Throughput optimization in high speed downlink packet access (HSDPA)," *IEEE Trans. Wireless Commun.*, vol. 10, no. 2, pp. 474–483, Feb. 2011.
[43] C. Yu, L. Yu, Y. Wu, Y. He, and Q. Lu, "Uplink scheduling and link adaptation for narrowband Internet of Things systems," *IEEE Access*, vol. 5, pp. 1724–1734, 2017.
[44] J. Francis and N. B. Mehta, "EESM-based link adaptation in point-to-point and multi-cell OFDM systems: Modeling and analysis," *IEEE Trans. Wireless Commun.*, vol. 13, no. 1, pp. 407–417, Jan. 2014.
[45] P. Kildal, A. Hussain, X. Chen, C. Orlenius, A. Skarbratt, J. Asberg, T. Svensson, and T. Eriksson, "Threshold receiver model for throughput of wireless devices with MIMO and frequency diversity measured in reverberation chamber," *IEEE Antennas Wireless Propag. Lett.*, vol. 10, pp. 1201–1204, 2011.
[46] S. Park, R. C. Daniels, and R. W. Heath, "Optimizing the target error rate for link adaptation," in *Proc. IEEE Global Commun. Conf. (GLOBECOM)*, Dec. 2015, pp. 1–6.
[47] X. Chen, W. Fan, P. Kyösti, L. Hentilä, and G. F. Pedersen, "Throughput modeling and validations for MIMO-OTA testing with arbitrary multipath," *IEEE Antennas Wireless Propag. Lett.*, vol. 17, no. 4, pp. 637–640, Apr. 2018.
[48] A. O. Laiyemo, H. Pennanen, P. Pirinen, and M. Latva-Aho, "Transmission strategies for throughput maximization in high-speed-train communications: From theoretical study to practical algorithms," *IEEE Trans. Veh. Technol.*, vol. 66, no. 4, pp. 2997–3011, Apr. 2017.
[49] D. Marabissi and R. Fantacci, "Heterogeneous public safety network architecture based on ran slicing," *IEEE Access*, vol. 5, pp. 24668–24677, 2017.
[50] J. Antoniou, V. Papadopoulou-Lesta, L. Libman, and A. Pitsillides, "Cooperative games among densely deployed WLAN access points," in *Game Theoretic Analysis of Congestion, Safety and Security: Networks, Air Traffic and Emergency Departments*, K. Hausken and J. Zhuang, Eds. 1st ed. Cham, Switzerland: Springer 2015, pp. 27–53.

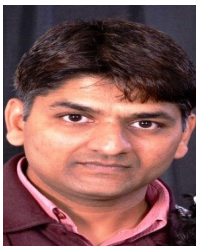

ANURAG VIJAY AGRAWAL (Member, IEEE) received the B.E. degree in electronics and communication engineering from MJP Rohilkhand University, Bareilly, Uttar Pradesh, India, in 2000, and the M.E. degree in electronics and communication engineering from Panjab University, Chandigarh, India, in 2010. He is currently pursuing the Ph.D. degree with the Department of Electronics and Communication Engineering, Indian Institute of Technology Roorkee, Roorkee, India.

His current research interests include MIMO/massive MIMO communications, digital predistortion, energy efficiency, transportation engineering, and high-speed train communications.

MEENAKSHI RAWAT (Member, IEEE) received the M.Sc. and Ph.D. degrees in electrical and computer engineering from the University of Calgary, Calgary, AB, Canada, in 2012.

From September 2012 to June 2013, she was a Postdoctoral Research Fellow with the University of Calgary. From July 2013 to June 2014, she was a Postdoctoral Project Researcher/Scientist with The Ohio State University. She is currently an Assistant Professor with Indian Institute of Technology Roorkee, Roorkee, India.

Dr. Rawat was a three-time recipient of the Research Production Award from the University of Calgary and the Best Paper Award from the 82nd and 83rd ARFTG Conference, in 2013 and 2014. She was a Workshop Co-Chair of the 82nd ARFTG Conference and a Session Co-Chair of mmWave and THz Designs for IMaRC 2014, India.